RSC Advances

PAPER

View Article Online
View Journal | View Issue

Cite this: *RSC Adv.*, 2025, **15**, 32553

Multifunctional hydrogels loaded with drugs for spinal cord injury repair

Jingjing Sun, *[a] Yuchen Cao,[b] Penmin Liu[b] and Jinfang Gao*[b]

Received 14th June 2025
Accepted 20th August 2025

DOI: 10.1039/d5ra04217h

rsc.li/rsc-advances

Spinal cord injury (SCI) constitutes a devastating neurological trauma that abolishes sensory and motor functions and triggers multiple complications, severely compromising patient quality of life. In response, we engineered a dynamic crosslinked hydrogel (CPFh-Mec) dedicated to SCI repair. The construct incorporates natural bioactives-chitosan (CTS), protocatechuic aldehyde (PA), and Fe(III) and functions as a scaffold for the neurorestorative drug mecobalamin (Mec). Dynamic covalent and hydrogen bonding confer exceptional adhesion, injectability, degradability, and autonomous self-healing. By profiling physicochemical properties, *in vitro* and *in vivo* biosafety, and reactive oxygen species (ROS)-scavenging efficacy, we achieve neuronal regeneration and motor recovery in SCI mice, offering a fresh paradigm for SCI biomaterial design.

1. Introduction

Spinal cord injury (SCI) ranks among the most devastating traumas of the nervous system. Typically triggered by traffic collisions or violent assaults, it carries a high probability of permanent disability and precipitates multi-system, multi-organ dysfunction.[1–3] Lifetime treatment costs per patient—dictated by lesion level and severity—range from tens of thousands to millions of dollars, imposing an immense burden on both individuals and national healthcare systems.[4] Current therapeutic strategies center on surgical decompression, pharmacologic intervention, and intensive rehabilitation.[5] Surgical intervention aims to restore the physiological and anatomical integrity of the spinal cord, reestablish its mechanical stability, and relieve compressive forces at the injured segment.

However, surgery remains inherently invasive, and consensus on the optimal timing of SCI operative intervention has yet to be established.[6,7] Current pharmacological regimens-encompassing methylprednisolone, dexamethasone, naloxone, erythropoietin, and neurotrophic factors-enhance neurological outcomes primarily by attenuating inflammatory mediator release and suppressing lipid peroxidation at the lesion site.[8] Nevertheless, the blood-spinal cord barrier markedly restricts drug penetration; conventional delivery routes (oral or moderate intravenous dosing) thus achieve only subtherapeutic concentrations at the injury focus.[9] Aggressive intravenous boluses, while potentially more effective, escalate the risks of gastrointestinal hemorrhage, wound infection, and other systemic complications, leaving this strategy clinically contentious and constrained.[10] Consequently, existing therapies merely palliate symptoms without addressing the underlying pathology. Compounding the challenge are the intricate pathophysiological cascades within the injured cord, the hostile local microenvironment, and the nervous system's limited intrinsic regenerative capacity, all of which render SCI treatment profoundly difficult.[11]

Driven by advances in tissue engineering and biomedicine, integrating biomaterial scaffolds with conductive substrates, living cells, and therapeutic agents has emerged as a highly promising strategy for spinal cord repair and neural regeneration.[12–14] Hydrogels-three-dimensional hydrophilic polymer networks—exhibit excellent biocompatibility, controllable degradability, low immunogenicity, and physicochemical versatility that closely mimics the native extracellular matrix, rendering them particularly attractive for spinal cord injury applications.[15–17] As versatile neural-tissue-engineering platforms, hydrogels can be engineered to deliver drugs or bioactive factors in a sustained manner, maintaining therapeutic concentrations locally, fostering cell proliferation, migration, and differentiation, and accelerating damaged-tissue restoration. In contrast, conventional administration routes frequently fail to regulate drug levels, and burst release can generate cytotoxic peaks that exacerbate tissue injury.[18] Consequently, hydrogel-based sustained-release systems have garnered widespread attention in recent years. Through diverse chemical and physical modifications, researchers have endowed hydrogels with tunable mechanical properties, dynamic responsiveness, and specialized biological functions, establishing them among the most compelling biomaterials for neural repair.[19,20]

Herein, we introduce a biosafe, dynamically double-crosslinked hydrogel fabricated from natural constituents-chitosan, protocatechuic aldehyde (PA), and Fe(III) without chemical modification, enabling scalable production for

[a]*Zhenjiang Mental Health Center, Zhenjiang, 212000, Jiangsu, China. E-mail: sjjjszj@163.com*

[b]*Third Hospital of Shanxi Medical University, Shanxi Bethune Hospital, Shanxi Academy of Medical Sciences, Tongji Shanxi Hospital, Taiyuan 030032, Shanxi, China. E-mail: gaojinfang@sxbqeh.com.cn*

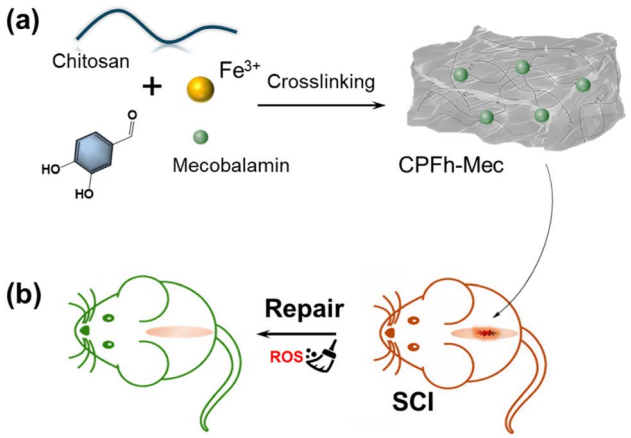

Fig. 1 Schematic illustration of the preparation process of multifunctional hydrogel (a) and its use for SCI repair (b).

clinical translation. The dynamic covalent and hydrogen bonds of this hydrogel endow it with superior adhesion, injectability, degradability, and self-healing capabilities, making it highly suitable for the spinal cord injury environment. The hydrogel provides sustained release of mecobalamin-the active form of vitamin B12 and a key mediator of nervous-system function-to drive neuronal growth and repair. In a mouse sciatic-nerve crush model, mecobalamin not only accelerated functional recovery, thickened myelinated-nerve fiber myelin sheaths and enlarged target-muscle fiber cross-sectional areas, but also mechanistically up-regulated GAP-43 mRNA and neurotrophic factors in the injured dorsal root ganglia, underscoring its capacity for potent neuroprotection and regeneration.[21,22] Meanwhile, the polyphenol PA in the hydrogel possesses antioxidant and anti-inflammatory properties, which can reduce free radicals and accelerate the repair of the spinal cord injury site.[23] This innovative platform not only addresses the complexities of spinal cord injury repair but also provides a multifunctional blueprint for the next generation of tissue repair biomaterials (Fig. 1).

2. Material and methods

2.1 Materials

Ferric chloride ($FeCl_3$), acetic acid, and protocatechuic aldehyde (PA) were purchased from Sinopharm Chemical Reagent, and the purity was chemically pure. Chitosan (CTS, a deacetylation degree of 90%, $M_w = 1.5 \times 10^5$ g mol^{-1}). Live–dead staining color development kit was purchased from Dalian Meilun Biotechnology Co. 4% paraformaldehyde fixative, bovine serum albumin (BSA), trypsin aqueous solution, PBS buffer was purchased from Biyuntian Biotechnology Co. NF-200, and GFAP were purchased from Abcam (UK).

2.2 Equipment and devices

The main equipment involved in the experiments were as follows: scanning electron microscope (SEM, SU8010, Hitachi), multifunctional enzyme labeling instrument (Epoch-2, BioTek), Animal gait analysis instrument (VisuGait, Shanghai Xinruan), Intelligent rheometer (MCR102, Anton Paar), UV-vis-NIR spectrometer (HL-2000, TS OPTICS).

2.3 Preparation of hydrogel CPFh-Mec

To prepare the hydrogel CPFh-Mec, 1.6 g of chitosan was dissolved in 80 mL of water, followed by the addition of 500 μL of acetic acid. The mixture was stirred overnight until the solution became clear. In a separate step, 45 mg of PA was dissolved in 3 mL of water, and 27 mg of $FeCl_3$ was dissolved in another 3 mL of water. After allowing the $FeCl_3$ solution to dissolve for 30 minutes, it was added dropwise to the PA solution to form a mixed aqueous solution. Then, 1 mL of the chitosan solution was combined with 200 μL of the mixed PA–$FeCl_3$ solution. Mecobalamin aqueous solution was subsequently added to this compound solution. The formation of a gel was observed, and the mixture was allowed to stand until the solution no longer flowed, resulting in the formation of the hydrogel CPFh-Mec.

2.4 Cytotoxicity assessment of hydrogels

The hydrogel was immersed in serum-free Dulbecco's modified eagle medium (DMEM) to obtain the hydrogel extract. The cells were spread evenly in 96-well plates. After the cells were attached to the wall, the cells were cultured by adding hydrogel extract containing 10% fetal bovine serum (FBS). The cells were stained with a cell viability kit to assess the cytotoxicity of the hydrogel. Cytotoxicity of the hydrogel was assessed by using a live/dead cell staining kit.

2.5 Construction of spinal cord injury model

To establish a mouse SCI model, a spinal cord impact device was used to strike the T10 segment of the mouse spinal cord. Animals were 8-week-old ICR male mice and the ICR mice were randomly and equally divided into 3 groups (control, saline, and CPFh-Mec). (1) Control group ($n = 6$): the group that underwent no surgery or treatment served as the control; (2) saline group ($n = 6$): saline was administered at the injury site after modeling; (3) CPFh-Mec group ($n = 6$): the pre-crosslinked hydrogel precursor was injected into the injury site. The skin was then sutured and disinfected with iodine tincture. After surgery, the mice were kept warm. Urination assistance was provided twice a day for the first three days and once a day thereafter.

2.6 Spinal cord tissue staining and pathologic analysis

The collected spinal cord tissue samples were subjected to paraffin embedding. The tissue samples to be embedded were first placed in liquid paraffin, and then cooled and frozen to turn the paraffin into a solid state for tissue fixation. Sections were made with a paraffin slicer at a thickness of 4–8 μm, and then placed on slides and soaked in warm water at 40 °C to fully stretch the tissue. Then, HE staining, LFB staining and immunofluorescence staining were performed for analysis. Spinal cord injury repair was assessed by immunofluorescence staining for NF-200, and GFAP. The relative fluorescence intensity of

NF-200, and GFAP was measured using Image J software to assess the expression levels of the corresponding fluorescent markers.

2.7 Statements for the animal experiments

In this work, all animal procedures were performed in accordance with the Guidelines for Care and Use of Laboratory Animals of Shanxi Medical University and approved by the Animal Ethics Committee of Shanxi Medical University. Surgery was performed in strict adherence to the principles of aseptic surgery to minimize the possibility of infection in the mice, and the wounds were treated locally with antibiotics to prevent infection.

3. Results and discussion

In the hydrogel preparation process, a weak polyphenol–metal interaction was first formed between PA with Fe(III), and then the aldehyde group of PA reacted with the amino group of chitosan to form a dynamic imine bond, which led to the formation of dynamically crosslinked hydrogels.[24,25] Fig. 2a showed the composition of the gel-forming ingredients and process for hydrogel CPFh-Mec, and screening various volume ratios of CTS to PA–Fe(III) revealed that robust hydrogels are obtained exclusively at 1 : 1, 5 : 1, and 10 : 1 (Fig. S1). Due to the time-dependent formation of imine bonds, the pre-gel aqueous solution can be extruded from the needle of a syringe (Fig. S2 and 2b), offering the possibility of injecting hydrogels into organisms. Besides, the storage modulus (G') and loss modulus (G'') of the sample were measured over time (Fig. 2e). In the initial stage, G' was lower than G'', indicating that the pre-gel CPFh aqueous solution containing mecobalamin was in a liquid state and had injectability. Subsequently, G' was equal to G'', indicating the occurrence of gelation and the beginning of the formation of the hydrogel CPFh-Mec. Lastly, the hydrogel can be injected *in situ* to fill the lesion cavity, solidifying within minutes to form a stable scaffold that releases mecobalamin for at least two weeks. The sustained release profile, coupled with the material's inherent antioxidant and anti-inflammatory properties, creates a permissive microenvironment for axonal regrowth and remyelination. As the hydrogel gradually degrades, it is replaced by newly regenerated neural tissue, leaving no permanent foreign body behind. G' was higher than G'', indicating that the gel solution had completed the transition from a liquid to a semi-solid state.[26] Hydrogel had both the stability of covalent bonds and the reversibility of non-covalent bonds, which can establish an intrinsic dynamic equilibrium of bond generation and dissociation in the hydrogel network, thus conferring the ability of self-repair to the hydrogel (Fig. 2c). Hydrogel had good adhesive properties and adhere well to metal, plastic, glass, and wood surfaces (Fig. 2d). Moreover, the viscosity of the hydrogel decreases with the increase of shear rate, indicating that the gel has shear-thinning properties (Fig. 2f). The strain sweep of the hydrogel shows (Fig. 2g) that an intersection between the storage modulus (G') and loss modulus (G'') occurred at a strain of 350%, which was the critical point indicating the collapse of the hydrogel network. Once

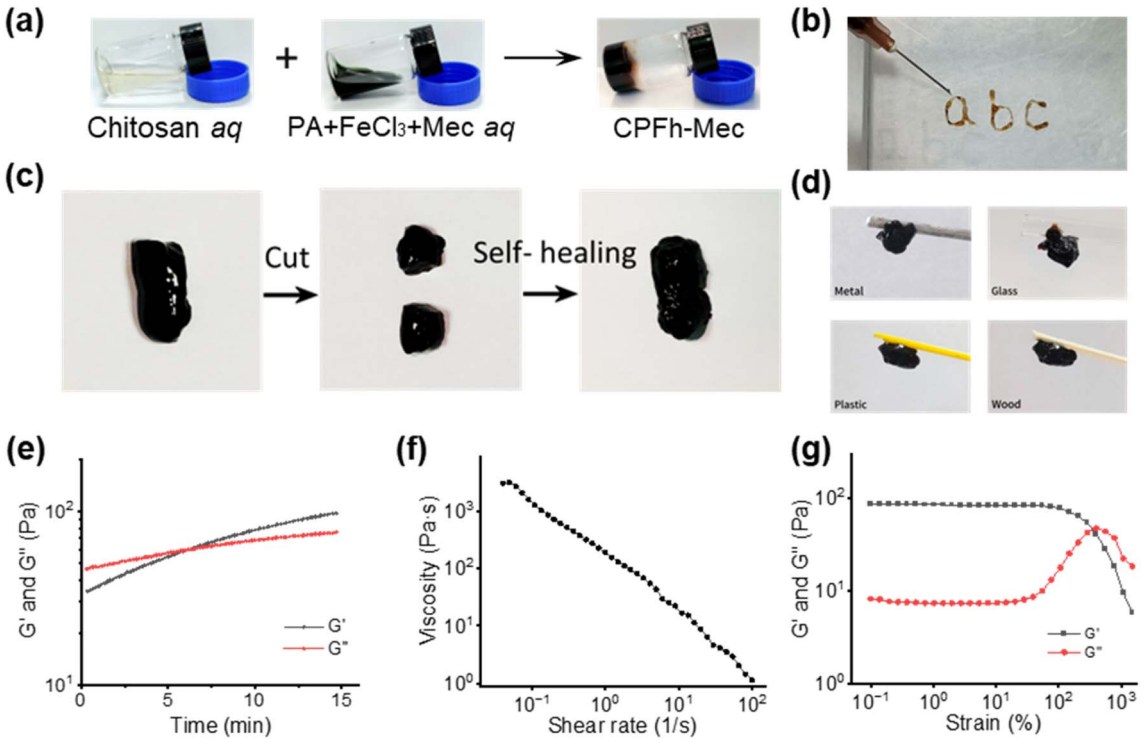

Fig. 2 (a) Schematic diagram of hydrogel preparation; (b) injectability, (c) self-healing and (d) adhesion of hydrogel CPFh-Mec; (e) the variation curve of the modulus of the injectable gel with time; (f) the shear-thinning properties of the hydrogel CPFh-Mec; (g) the strain sweep of the hydrogel CPFh-Mec with the strain ranging from 0.1% to 1500%.

the strain exceeds this critical value, G' dropped sharply.[27] Besides, CPFh-Mec showed significant disintegration after 7 days, indicating good degradation properties (Fig. S3).

The surface morphology of hydrogel was observed by scanning electron microscopy. The hydrogels showed a loose and porous structure with a void size of 20–60 μm (Fig. 3a). SEM mapping of CPFh-Mec revealed the presence of C, O, Fe and N elements (Fig. 3b). Moreover, the live/dead cell staining confirmed the good cytocompatibility of the hydrogel (Fig. 3c and e), and the cells showed green fluorescence (live cells). High intracellular ROS induces continuous apoptosis and stimulates the activation of inflammatory cells, therefore, improving the high intracellular and extracellular ROS is conducive to the rapid repair of the damaged area. As shown in Fig. S4, 3d and f, CPFh-Mec effectively scavenges intracellular ROS generated by H_2O_2; this capacity stems from the intrinsic antioxidant activity of protocatechuic aldehyde, a polyphenol that rapidly reduces hydrogen peroxide. Moreover, prolonged incubation enriches the leachate with additional active constituents released from the hydrogel, progressively enhancing its H_2O_2-eliminating efficacy over time.

To evaluate the antioxidant properties of CPFh-Mec, this study explored its ability to scavenge the free radicals DPPH/ABTS. As shown in Fig. 4a and b, the changes in DPPH/ABTS free radical signals indicate that the scavenging ability of CPFh-Mec against DPPH/ABTS free radicals is concentration-dependent. With the increase in CPFh-Mec concentration, the free radical scavenging ability also increases. This is due to the presence of antioxidant polyphenolic substances in the hydrogel. SOD, as an important antioxidant enzyme in the body, is mainly responsible for scavenging superoxide radicals.[28,29] Synthesizing nanozymes with SOD activity is of great significance for the treatment of oxidative stress-related diseases. As shown in Fig. 4c, the SOD activity of CPFh-Mec was concentration-dependent. With the increase in CPFh-Mec concentration, the SOD activity also increases.

To detect the neuroprotective effects of CPFh-Mec on SCI mice, double fluorescence labeling was used for NF-200 (green) and GFAP (red) to observe the number of astrocytes and the extension of axons. NF-200 is a neurofilament that provides structural support to axons and regulates axon diameter, while GFAP marks the activation of astrocytes.[30,31] As shown in Fig. S5, 5a–c, in the saline group, the expression of NF-200-positive axons was very low in the lesion area, and the expression of GFAP was also relatively low. This indicates that there was severe axonal damage and a reduction in astrocytes in the spinal cord tissue of the saline group. In contrast, the expression of NF-200 and GFAP increased in the lesion area of the CPFh-Mec group. This suggests that during the subacute phase of SCI, CPFh-Mec is beneficial for the recovery of damaged spinal cord nerves. CPFh-Mec can promote astrocyte proliferation and axon growth, showing significant neuroprotective effects on the injured site after SCI.

The histological changes in spinal cord tissues were studied using H&E staining. As shown in the left image of Fig. 6a, the control group exhibited well-organized and intact normal mouse spinal cord tissue. In contrast, the saline group displayed the lowest degree of recovery, with the spinal cord

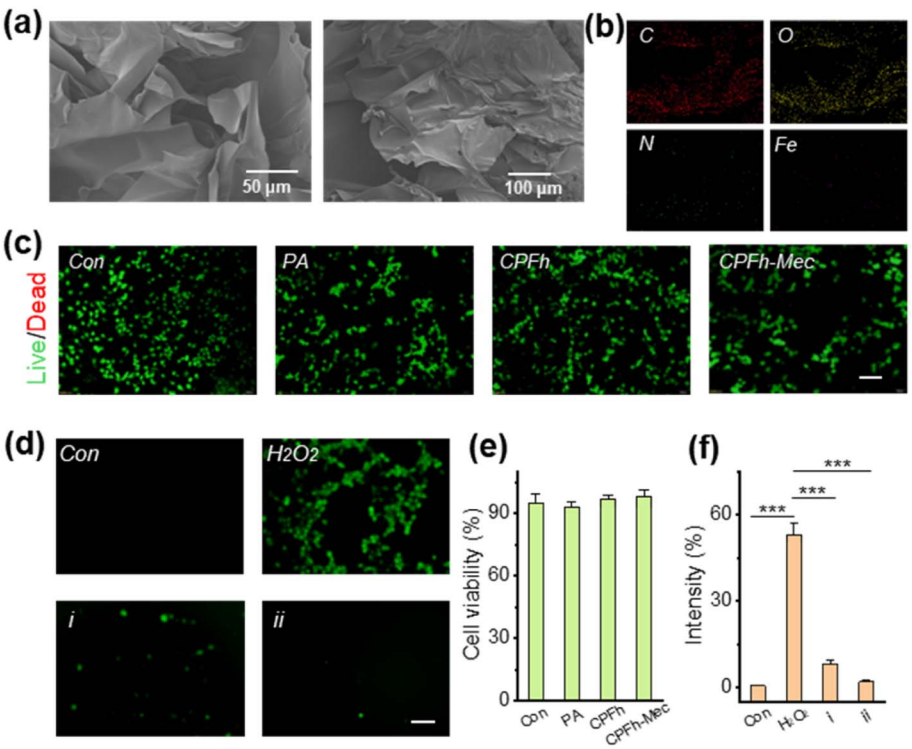

Fig. 3 (a) Scanning Electron Microscope (SEM) and (b) elemental distribution of CPFh-Mec; (c) cytocompatibility and (e) cell viability of control, PA, hydrogels CPFh and CPFh-Mec (scale bar: 300 μm); (d) fluorescence images of intracellular H_2O_2 and (f) the relative intensity before and after CPFh-Mec treatment (i and ii: hydrogel leachate collected after 1 and 3 days, scale bar: 200 μm). All data were presented as mean ± SD, $n = 3$. ***$p < 0.001$.

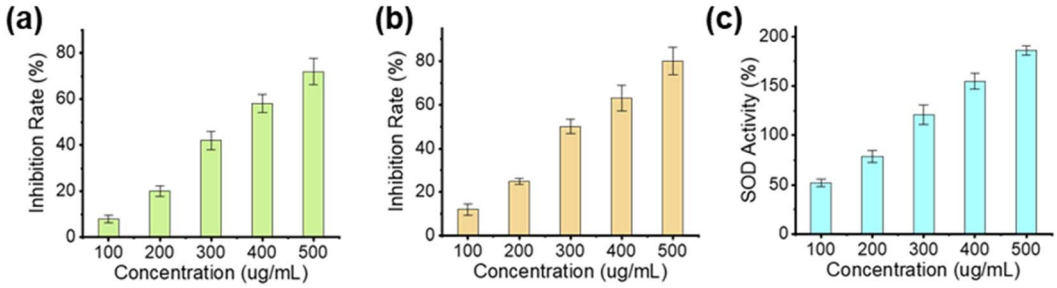

Fig. 4 Scavenging ability of CPFh-Mec for free radical DPPH (a) and ABTS (b); (c) SOD-like enzyme activity of CPFh-Mec. All data were presented as mean ± SD, $n = 3$.

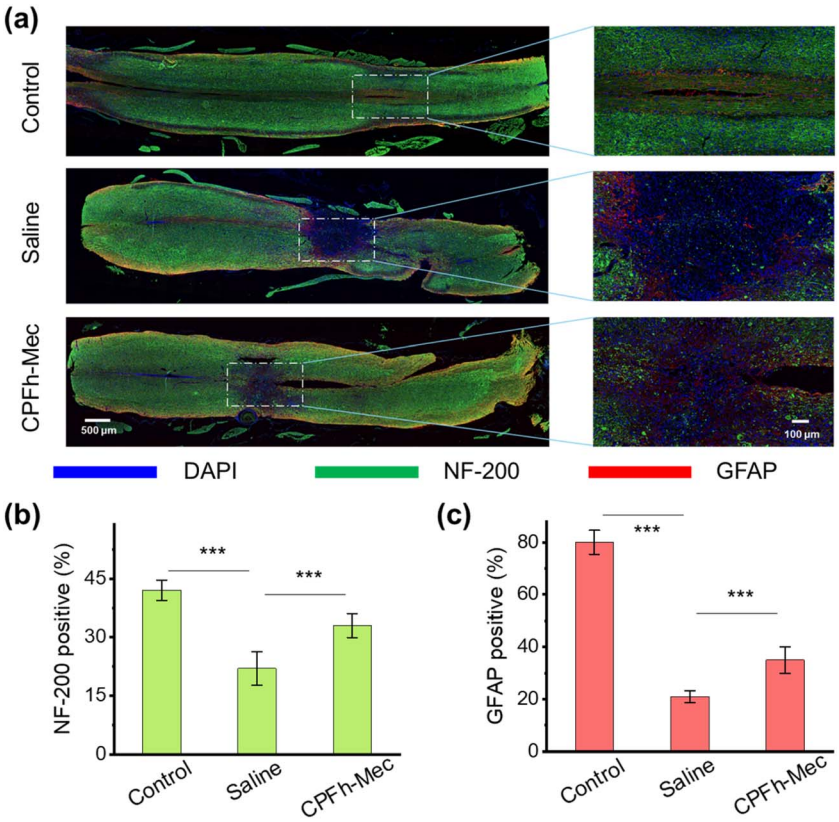

Fig. 5 (a) NF-200 and GFAP immunofluorescence stained image; quantitative analysis of NF-200 (b) and GFAP (c) positive cell. All data were presented as mean ± SD, $n = 3$. ***$p < 0.001$.

lacking continuity and integrity. However, treatment with CPFh-Mec improved the continuity and integrity of the spinal cord. Meanwhile, the right image (Fig. 6a) showed that the SCI area in the CPFh-Mec group had significantly fewer inflammatory cells compared with the saline group. To evaluate whether CPFh-Mec could exert a protective effect on demyelination after SCI, the extent of axonal demyelination in the lesion area was assessed using LFB staining. As shown in Fig. 6b, the spinal cord of the saline group mice showed significant demyelination. In contrast, the CPFh-Mec group had more myelin sheaths preserved. In summary, the results of LFB staining demonstrated the positive effect of CPFh-Mec treatment on demyelination.[32]

To verify these results, a gait analyzer was further employed to assess the motor function of mice after SCI, and gait pressure footprint maps of mice in each group were obtained (Fig. 6c). The results of the usable parameters measured by the gait analyzer are shown in Fig. 6d–g. The average pressure value of the left forepaw footprint in the saline group was the highest (Fig. 6d). This was because the hindlimb motor function of mice in the saline group was restricted after SCI, and the forelimbs became the main force-generating limbs. The results of the average pressure of the right front paw footprint in Fig. 6e were similar to those in Fig. 6d. Meanwhile, Fig. 6f and g showed that the average footprint area ratio of the left and right forepaws in the saline group was higher than that in the control and CPFh-

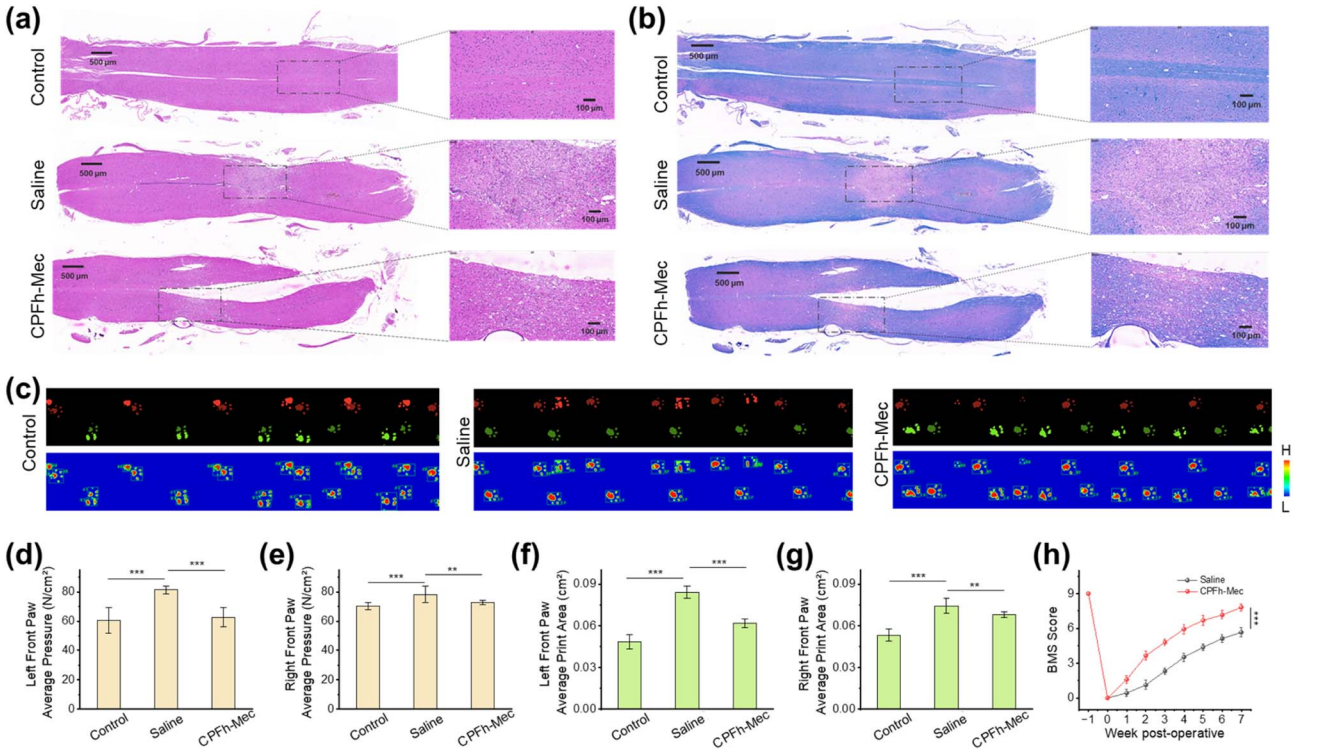

Fig. 6 (a) HE and (b) LFB stained image of mouse spinal cord tissue; (c) mouse paw footprints and pressure footprint images; the average pressure of footprints corresponding to the left (d) and right (e) forelimbs of mice; the average footprint area corresponding to the left (f) and right (g) forelimbs of mice; quantitative analysis of collagen stained areas; (h) BMS score from 0 to 7 weeks after SCI. All data were presented as mean ± SD, $n = 3$. $^{**}p < 0.01$, $^{***}p < 0.001$.

Mec groups. This was due to the increased contact area of the forelimbs in the saline group mice, which became the main force-generating limbs. These results further demonstrate that CPFh-Mec played a positive therapeutic role in improving and restoring the motor function of mice. As shown in Fig. 6h, immediately after SCI modeling, all the modeled mice had a BMS score of 0, indicating complete loss of hindlimb motor function. On week 2 after SCI, all the modeled mice began to show varying degrees of hindlimb motor function recovery, with BMS scores gradually increasing. By week 6 after SCI, compared with the saline group, mice treated with CPFh-Mec exhibited better motor function recovery.

4. Conclusions

In this work, a dynamic double-crosslinked hydrogel was fabricated *via* Schiff-base chemistry and polyphenol–metal coordination; the resultant carrier was loaded with the neuroreparative agent methylcobalamin to yield the multifunctional construct CPFh-Mec. Comprehensive physicochemical characterization confirmed outstanding adhesion, injectability, and autonomous self-healing. In a mouse model of spinal cord injury, CPFh-Mec exhibited robust bioactivity, accelerating cellular proliferation and growth. Immunofluorescence revealed marked enhancement of astrocyte proliferation and axonal extension, driving significant neural regeneration. The synergistic interplay of these effects underpins the hydrogel's capacity for effective spinal cord repair.

Conflicts of interest

There are no conflicts to declare.

Data availability

Gelation behavior of chitosan with PA-Fe(III) at different volume ratios; Different compositional gelation processes; CPFh-Mec hydrogel stability testing over one week; Photothermal properties of hydrogel; NF-200 and GFAP immunofluorescence stained image. The authors confirm that the data supporting the findings of this study are available within the article and its SI. See DOI: **https://doi.org/10.1039/d5ra04217h**.

Acknowledgements

This work has been financially supported by Shanxi Province Clinical Research Center for Dermatologic and Immunologic Diseases (Rheumatic diseases) Scientific Research Project (LYZX-202302).

References

1 G. B. Gao, J. J. Li, Y. M. Ma, M. Xie, J. X. Luo, K. Wang, J. Ouyang, H. S. Lin and Z. S. Ji, Dual-responsive multifunctional silica nanoparticles with repaired mitochondrial functions for efficient alleviation of spinal cord injury, *Exploration*, 2025, **5**, 270012.

2 M. D. Sunshine, V. E. Bindi, B. L. Nguyen, V. Doerr, F. P. Boeno, V. Chandran, A. J. Smuder and D. D. Fuller, Oxygen therapy attenuates neuroinflammation after spinal cord injury, *J. Neuroinflammation*, 2023, **20**, 303.
3 B. Guan, Y. Fan, R. Zheng, R. Fu, L. Yao, W. Wang, G. Li, L. Chen, H. Zhou and S. Feng, A critical appraisal of clinical practice guidelines on pharmacological treatments for spinal cord injury, *Spine J.*, 2023, **23**(3), 392.
4 M. Patel, Y. Li, J. Anderson, S. Castro-Pedrido, R. Skinner, S. Lei, Z. Finkel, B. Rodriguez, F. Esteban, K. B. Lee, Y. L. Lyu and L. Cai, Gsx1 promotes locomotor functional recovery after spinal cord injury, *Mol. Ther.*, 2021, **29**, 2469.
5 R. D. Bartlett, S. Burley, M. Ip, J. B. Phillips and D. Choi, Cell therapies for spinal cord injury: Trends and challenges of current clinical trials, *Neurosurgery*, 2020, **87**, 456.
6 C. Y. Adegeest, P. V. Wengel and W. C. Peul, Traumatic spinal cord injury: Acute phase treatment in critical care, *Curr. Opin. Crit. Care*, 2023, **29**, 659.
7 M. Piazza and J. Schuster, Timing of surgery after spinal cord injury, *Neurosurg. Clin.*, 2017, **28**, 31.
8 X. Hu, W. Xu and Y. Ren, Spinal cord injury: molecular mechanisms and therapeutic interventions, *Signal Transduction Targeted Ther.*, 2023, **8**, 245.
9 A. Akhtar, A. Andleeb and T. S. Waris, Neuro degenerative diseases and effective drug delivery: A review of challenges and novel therapeutics, *J. Controlled Release*, 2021, **330**, 1152.
10 S. H. Choi, C. Sung and D. R. Heo, Incidence of acute spinal cord injury and associated complications of methylprednisolone therapy: A national population-based study in South Korea, *Spinal Cord*, 2020, **58**, 232.
11 S. Gupta, J. Dhawan and M. A. McColl, Use and costs of nonprescription medications among people with spinal cord injury, *Arch. Phys. Med. Rehabil.*, 2022, **103**, 127.
12 D. S. Zhang, R. He, Y. Qu, C. He and B. Y. Chu, Application of biomaterials in cardiac tissue engineering: Current status and prospects, *MedComm: Biomater. Appl.*, 2024, **3**, e103.
13 S. Kumar, R. Malviya and S. Sundram, Management of peripheral nerve injuries using natural based biomaterials and their derivatives: Advances and prospective, *MedComm: Biomater. Appl.*, 2024, **3**, e72.
14 C. L. Cai, T. Wang, Y. X. Zhang, C. H. Lin, Z. Q. Feng, Y. Cai and N. Y. He, Integrated implantable triboelectric charge collector for nerve repair, *Chin. Chem. Lett.*, 2025, 111087.
15 Y. Wang, H. Lv and X. Chao, Multimodal therapy strategies based on hydrogels for the repair of spinal cord injury, *Mil. Med. Res.*, 2022, **9**, 1.
16 E. A. Kiyotake, M. D. Martin and M. S. Detamore, Regenerative rehabilitation with conductive biomaterials for spinal cord injury, *Acta Biomater.*, 2022, **139**, 43.
17 S. Cheng, M. Pan, D. R. Hu, R. X. Han, L. Li, Z. W. Bei, Y. C. Li, A. Sun and Z. Y. Qian, Adhesive chitosan-based hydrogel assisted with photothermal antibacterial property to prompt mice infected skin wound healing, *Chin. Chem. Lett.*, 2023, **34**, 108276.
18 R. Shultz and Y. Zhong, Hydrogel-based local drug delivery strategies for spinal cord repair, *Neural Regener. Res.*, 2021, **16**, 247.
19 L. Zhou, Z. Wang and D. Chen, An injectable and photocurable methacrylate-silk fibroin hydrogel loaded with bFGF for spinal cord regeneration, *Mater. Des.*, 2022, **217**, 110670.
20 H. Shen, B. Xu and C. Yang, A DAMP-scavenging, IL-10-releasing hydrogel promotes neural regeneration and motor function recovery after spinal cord injury, *Biomaterials*, 2022, **280**, 121279.
21 L. Gan, J. Wang, Y. Zhang, X. Wang, H. Li and Y. Guo, Mecobalamin promotes nerve regeneration in a rat sciatic-nerve crush model by up-regulating GAP-43 and neurotrophic factors, *Neural Regener. Res.*, 2014, **9**, 1979.
22 K. Okada, H. Tanaka, T. Murase and H. Yoshikawa, Mecobalamin accelerates functional recovery and increases myelinated fiber size after sciatic-nerve injury in mice, *Exp. Neurol.*, 2010, **222**, 191.
23 A. Joorabloo and T. Q. Liu, Recent advances in reactive oxygen species scavenging nanomaterials for wound healing, *Exploration*, 2024, **4**, 20230066.
24 S. Talebian, M. Mehrali, M. Hasany, M. Nikkhah, G. Akbari and A. Orive, Self-healing hydrogels: the next paradigm shift in tissue engineering, *Adv. Sci.*, 2019, **6**, 1801664.
25 Y. Yang and M. W. Urban, Self-healing polymeric materials, *Chem. Soc. Rev.*, 2013, **42**, 7446.
26 H. He, Z. Y. Fei, C. Wang, X. Lu and T. L. Guo, Bioadhesive injectable hydrogel with phenolic carbon quantum dot supported Pd single atom nanozymes as a localized immunomodulation niche for cancer catalytic immunotherapy, *Biomaterials*, 2022, **280**, 121272.
27 Y. Q. Liang, Z. L. Li, Y. Huang, R. Yu and B. L. Guo, Dual-dynamic-bond cross-linked antibacterial adhesive hydrogel sealants with on-demand removability for post-wound-closure and infected wound healing, *ACS Nano*, 2021, **15**, 7078.
28 Y. Huang, J. Ren and X. Qu, Nanozymes: classification, catalytic mechanisms, activity regulation, and applications, *Chem. Rev.*, 2019, **119**, 4357.
29 L. Shang, Y. Yu, Y. Jiang, X. Liu, N. Sui, D. Yang and Z. Zhu, Ultrasound-augmented multienzyme-like nanozyme hydrogel spray for promoting diabetic wound healing, *ACS Nano*, 2023, **17**, 15962.
30 F. Feng, X. Y. Song, Z. Tan, Y. J. Tu and L. M. He, Cooperative assembly of a designer peptide and silk fibroin into hybrid nanofiber gels for neural regeneration after spinal cord injury, *Sci. Adv.*, 2023, **9**, eadg0234.
31 Y. F. Wang, T. F. Zhao, Y. R. Jiao and K. Xu, Silicate nanoplatelets promotes neuronal differentiation of neural stem cells and restoration of spinal cord injury, *Adv. Healthcare Mater.*, 2023, **5**, 2203051.
32 J. Meng, J. J. Sun, J. L. Kang, S. L. Ren, M. M. Xu, R. Z. Li, X. H. Zhao, Y. T. Yuan, L. Xin and R. P. Zhang, Multifunctional hydrogels loaded with tellurium nanozyme for spinal cord injury repair, *Mater. Today Bio*, 2024, **29**, 101339.